ORIGINAL PAPER

NON-INVASIVE ANALYTICAL TECHNIQUES APPLIED ON PIGMENTS CHARACTERIZATION OF ANCIENT BIVALVE SHELLS

IOANA DANIELA DULAMA[1], CRISTIANA RADULESCU[1,2,3*], IOAN ALIN BUCURICA[1*], SOFIA SLAMNOIU-TEODORESCU[1], RALUCA MARIA STIRBESCU[1], VALENTINA VOINEA[4]; VALENTIN RADU[5]; MONICA MARGARIT[6]

Manuscript received: 11.09.2021; Accepted paper: 22.10.2021;
Published online: 30.12.2021.

Abstract. *In this paper was studied eight bivalve shells (with pigments traces) collected from Cheia archaeological site (Eneolitihic site, dated between the end of the 6th millennium and the beginning of the 5th millennium cal BC, Romania), in order to established correlations related to morphology, composition, longevity and belonging to the archaeological site of these shells. The samples (pigments and shells) were investigated, from morphological and chemical composition point of view, by optical microscopy, scanning electron microscopy coupled with energy dispersive spectroscopy (SEM-EDS), and attenuated total reflectance - Fourier transform infrared (ATR-FTIR) spectroscopy, respectively. Principal component analysis (PCA) and cluster analysis (CA) were carry out using IBM SPSS Statistics software to assess the similarities between the investigated samples*

Keywords: *pigment; bivalve shells; SEM-EDS; FTIR; statistical analysis.*

1. INTRODUCTION

Typically, the bivalve shells are a calcareous exoskeleton [1, 2] which has a well-established role, namely protects the soft parts of the phylum Mollusca (e.g. clams, snails, and octopus), from predators and mechanical damage. Thus, bivalves are part of the mollusk body and possess two shells, as equal sides, that are joined by a ligament [3]. Several studies [4-7] shown that the composition of shell is from calcium carbonate precipitated into an organic matrix [8, 9]. Taking into account the chemical composition of bivalve shells, it can be concluded that they are actually, inorganic-organic nanocomposites, which from material properties point of view, outperform their purely inorganic mineral counterparts [5, 6]. Therefore, the calcareous matrix of bivalve shells contain an inorganic phase, a polymorph form of calcium carbonate, and an organic phase mainly formed by chitin and/or protein [5, 6], responsible for enhanced mechanical properties [6]. Due to their compositional structure, the bivalve shells have different applications as safer, eco-friendly, and lower cost biosorbents [10, 11] in remove dyes of dyes from wastewater resulted from textile, paper, paint, food, pharmaceutical and cosmetic industries. On the other hand, the elements concentration (i.e.

[1] Valahia University of Targoviste, Institute of Multidisciplinary Research for Science and Technology, 130004 Targoviste, Romania.
[2] Valahia University of Targoviste, Faculty of Science and Arts, 130004 Targoviste, Romania.
[3] University Politehnica of Bucharest, Doctoral School of Biotechnical Systems Engineering, Bucharest, Romania
[4] Museum of National History and Archeology, 900178 Constanta, Romania.
[5] National Museum of Romanian History, 030026 Bucharest, Romania.
[6] Valahia University of Targoviste, Faculty of Humanities, 130105 Targoviste, Romania.
[*] *Corresponding authors: bucurica_alin@yahoo.com; radulescucristiana@yahoo.com.*

strontium, boron, hydrogen, oxygen, barium, nitrogen, carbon) in bivalve shells might provide suitable proxies for pH changes [12], salinity [13], freshwater pulses [14], phytoplankton dynamics [15], and not at last provide information on anthropogenic pollution [16]. However, several studies shown that the shell chemistry is not a real bioindicator for climate change [17, 18] and actual pollution [19, 20].

For many bivalves' species, the outside surface of shells is covered by a periostacum, with an important role both in the growth and maintaining of the exoskeleton, most often, being considered a good biopolymer [19, 21, 22], with large application in jewelry, household utensils, and ornaments fabrication.

Related to the relationship between size and longevity in the fresh water of mussels, Haag and Rypel demonstrated that the longevity (e.g. depending of taxonomic class the life exceed 400 years) is strongly influenced by bivalve shell thickness, suggesting that their thickness may provide greater resistance to different hazards, such as predator or variation of temperature [23]. Since ancient times, it is very clear [24-26] that these shells have been used as household or storage utensils in peoples daily live. Such shells used hundreds of years ago, discovered in different archaeological sites around of the world, have led to amazing conclusions [27, 28] about the actual age of the sites, related to radiocarbon dating [29].

In an important Eneolithic archaeological site in Romania, named Cheia, situated in the western of Black Sea (Dobrogea Province) (Fig. 1) near of Casimcea River, a few bivalves' shells among other objects that have highlighted the traces of human settlements were discovered. Radiocarbon data includes the archaeological site at the end of the 6th millennium and the beginning of the 5th millennium BC (5200-4700 BC), which corresponds to Hamangia Culture Phase III or Early Eneolithic [24, 25, 30, 31]. The geo-physical prospects show that the settlement occupied a large area, about 7 ha. The housing areas consists in surface dwellings, annexed constructions, pits and outside storage areas; also included spaces for animals. In the researched area (about 700 m^2) were identified two houses, partially overlapped. The animal paleo-economy is dominated by husbandry. Hunting and seasonally exploitation of aquatic resources are also sources of food [32-36].

Figure 1. Cheia settlement, Hamangia culture.

In this article, it was investigated the pigments and shells using non-invasive analytical techniques (e.g., optical microscopy, SEM-EDS, ATR-FTIR, and Raman spectroscopy) and the elemental composition determined by EDS were used in statistical analysis in order to investigate the similarities between samples.

2. MATERIALS AND METHODS

For analysis, 101 valves were retained which had various wear traces (93 items) or residues (8 items). Their determination revealed that one valve belonged to the species *Anodonta* sp., 5 items of *Unio pictorum* species, 40 items of *Unio tumidus* species and one item of *Unio crassus* species. Due to the increased fragmentarity, 54 valves were classified only at the genus level (*Unio* sp.). Experimental studies have shown that valves with wear traces could be used to process ceramics [37]. On eight of these valves, it was possible to identify spots of red pigments (Fig. 2) what will be the subject of this study. The bivalve shells were collected from Cheia archaeological site (Constanța County, Romania). From each shell were separated the colored residue (samples were coded as P1-P8) and a small piece from the clean shell (samples were coded as S1-S8).

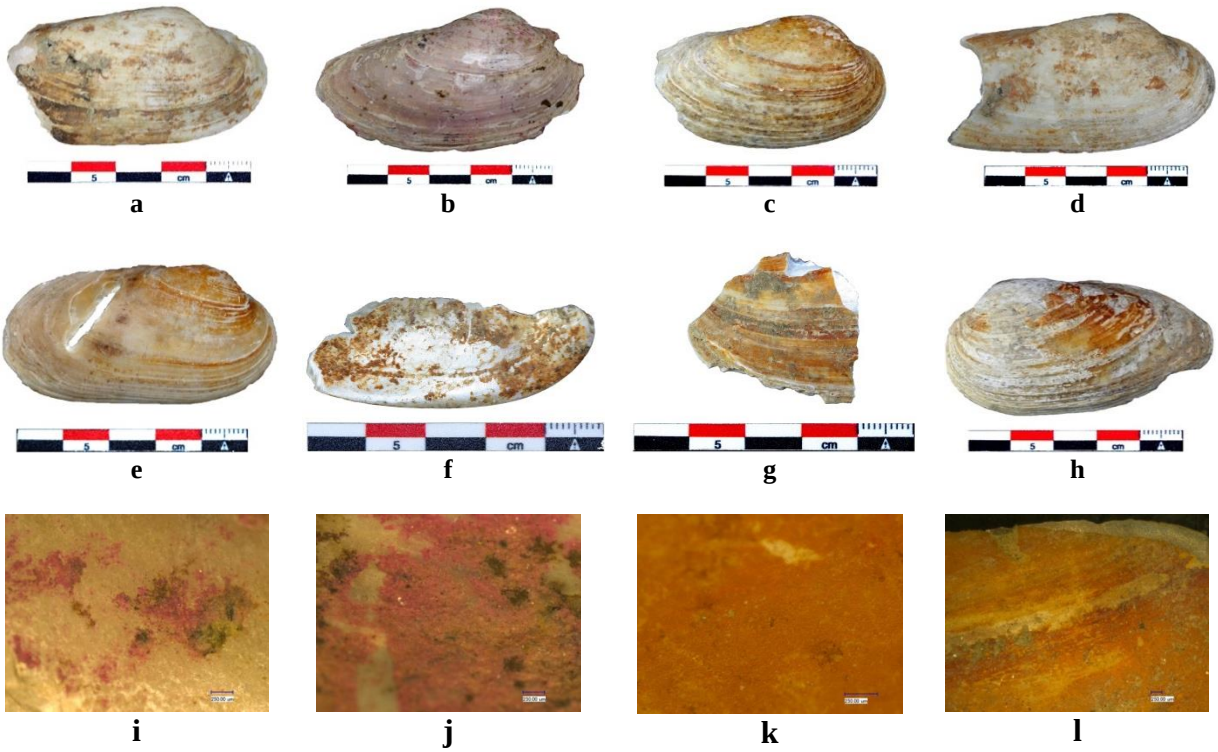

Figure 2. Bivalve shell samples with pigments traces: a) and d) *Unio pictorum* (painter mussel); b), c) and h) *Unio tumidus* (swollen river mussel); e) and f) *Unio crassus* (thick-shelled river mussel); g) *Anodonta cygnea* (swan mussel); i)-l) optical microscopy images of red pigment spots.

The analyzed species of bivalves are characteristic of the fresh waters and the lower area of the Danube River. *Unio pictorum* and *Unio tumidus* live in the rivers especially in areas with low water current and sandy-muddy bottom, or in the lakes permanently supplied by a river. *Unio crassus* live predominantly in rivers with strong currents, sandy bottom and

well oxygenated waters, while *Anodonta cygnaea* is found in rivers with low water current and lakes.

In the first step, the methodology used in this study relied on macroscopic and microscopic analysis of the technological, use-wear traces and pigment spots present on the archaeological items. For this purpose, the valves were analyzed with a Keyence VHX-600 digital microscope (Keyence Corp., USA), with magnifications ranging from 30x to 150x, the images being taken using an embedded camera.

Microstructural investigation of the samples was performed by scanning electron microscopy (SEM) using the emission scanning electron microscope SU-70 (Hitachi Ltd, Tokyo, Japan). Phase compositions were performed by energy dispersive X-ray (EDS) spectroscopy elemental analyses using UltrDry EDS (Thermo Fisher Scientific, Waltham, MA, USA) coupled at SEM system The samples morphology was obtained at following operation conditions: high vacuum = 10^{-8} Pa, accelerating voltage =1 kV (resolution 1.6 nm), working distance = 18.0 – 19.5 mm, while for EDS analyzes the acceleration voltage was increased up to10 kV. Fourier transform infrared spectroscopy was used to analyse the characteristic molecular absorption of infrared light, to determine structure of organic or inorganic compounds, typically in the range of 4000 – 400 cm^{-1}, with 0.2 cm^{-1} spectral resolution, 0.1% T accuracy and 32 scans. Therefore, FTIR spectra were recorded by using a Vertex 80v spectrometer (Bruker, Ettlingen, Germany) equipped with Attenuated Total Reflectance (ATR) accessory. Data analysis was performed using IBM SPSS (Statistical Package for the Social Science) Statistics (software version 21) for MS Windows.

3. RESULTS AND DISCUSSION

The SEM morphological investigation of P1 pigment sample reveal that it consists in large tetrahedral / acicular structures (Fig. 3a, Fig. 3b) with ~20x20 μm^2 base area and height up to 100 μm; these crystallites are embedded in a fine powder matrix (Fig. 3a, Fig. 3c). The EDS data reveal that the acicular part contains only carbon, oxygen, aluminum (<1%) and calcium and offer the first ascertainment on the nature of the principal mineral composing the pigments, that is calcium carbonate.

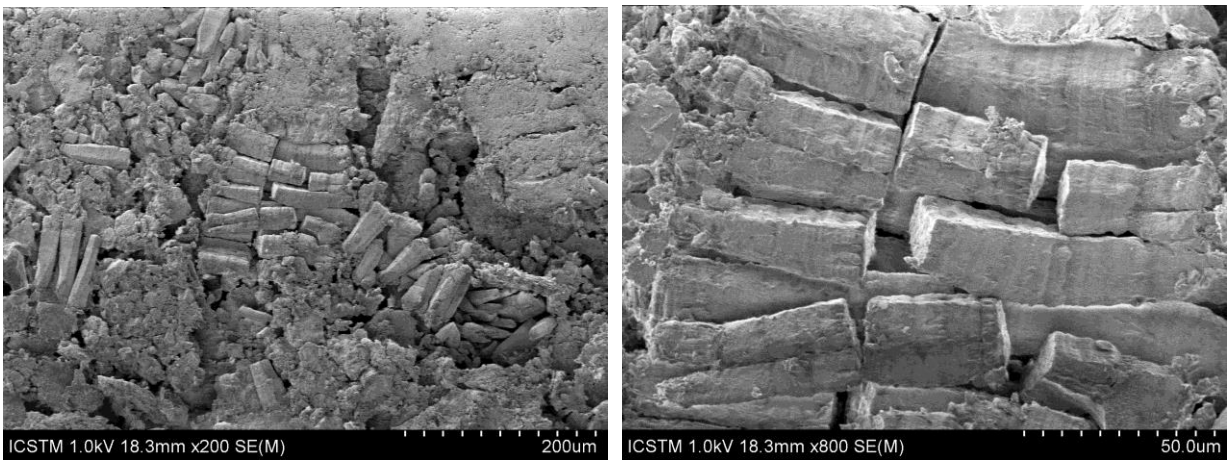

a) **b)**

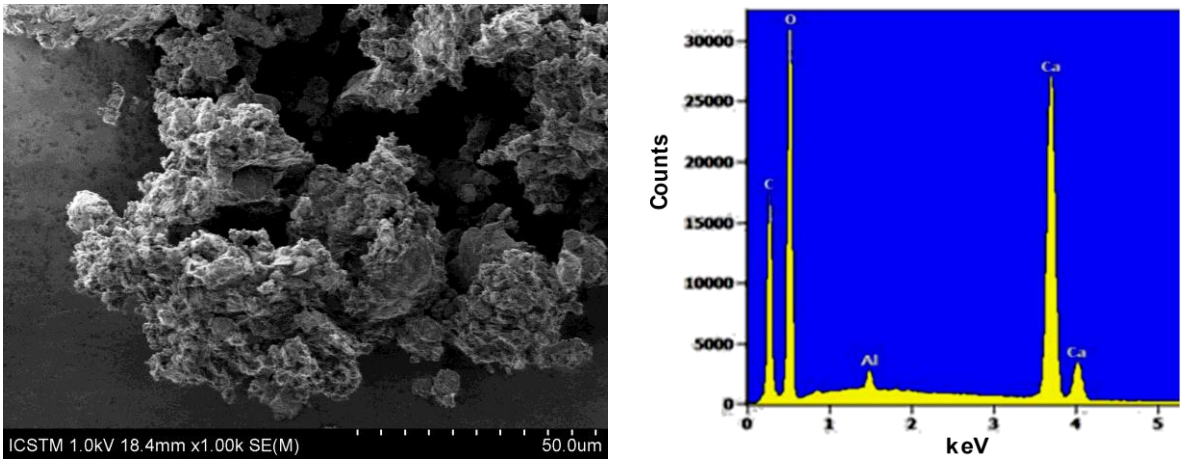

c) **d)**

Figure 3. Scanning electron micrographs (SEM) of pigment P1: a) general view; b) acicular structures; c) fine powder matrix. d) EDS spectrum of acicular crystallites present in P1.

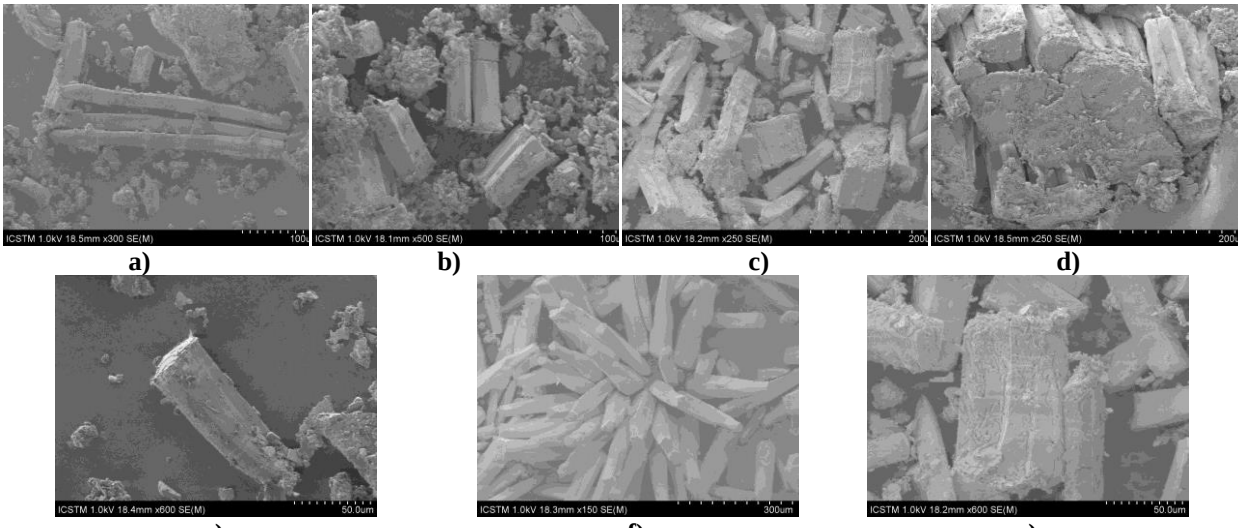

a) **b)** **c)** **d)**

e) **f)** **g)**

Figure 4. Scanning electron micrographs (SEM) of pigments: a) P2; b) P3; c) P4; d) P5; e) P6; f) P7; g) P8.

The structure described above was observed on all pigment samples with few minor differences: in P2 (Fig. 4a) the acicular crystallites are larger than those of P1 (h ≈ 200 μm) and the powder represents the principal structure of the sample; P3-P6 samples (Figs. 4b-e) show similarities in terms of crystallite size and acicular / powder ratio; in P7 sample (Fig. 4f) can be observed the sharp shapes, while P8 sample (Fig. 4g) appears to be affected by some microorganisms. The SEM morphology images (Figs. 5a-h) on internal layer of shell samples highlight a simple lamellar structure with sharp corners and thin layers. The acicular crystallites observed in previous figures (Figs. 3a-b; Figs. 4a-g) correspond to the external structure of shells. All data are in accordance with other studies [38].

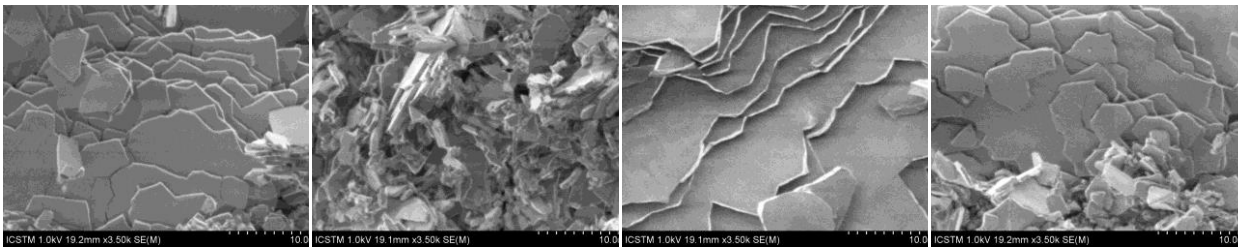

a) **b)** **c)** **d)**

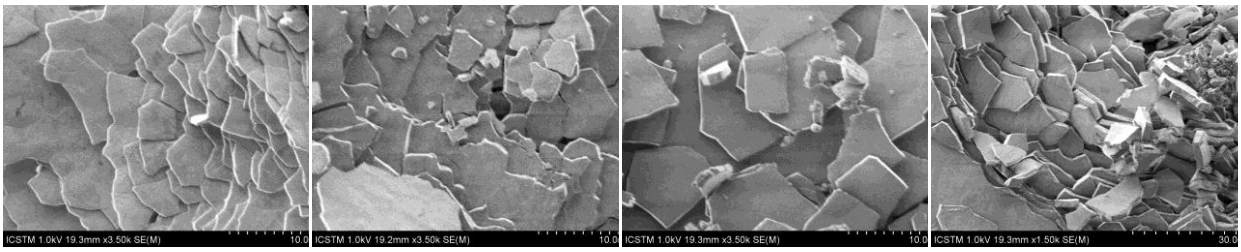

e) f) g) h)

Figure 5. Scanning electron micrographs (SEM) of shell samples: a) S1; b) S2; c) S3; d) S4; e) S5; f) S6; g) S7; h) S8.

The energy dispersive X-ray spectroscopy of the shell samples (i.e. S1-S8) reveals that the major constituents are C, O, Al, and Ca, but in few samples were observed small amount of Na, Si, K or Ni. As expected, the elemental composition of pigment samples (i.e. P1-P8) was more complex than the shells and, except the major constituents, other elements such as Mg, K, Ti, Fe, and Ir were identified and quantified. All data are presented in Table 1, the elemental concentration being expressed as both mass and atomic percent, normalized to 100%.

Table 1. Elemental composition, expressed as wt.%±standard deviation% and at.% ± standard deviation%, normalized to 100%, of pigment (Px)and shell samples (Sx).

		C	O	Na	Mg	Al	Si	P	K	Ca	Ti	Fe	Ir	Ni
P1	wt. [%]	6.28± 0.07	51.34 ±0.26	-	1.33± 0.03	6.75± 0.05	16.22 ±0.08	-	2.83± 0.07	9.60± 0.11	-	5.20± 0.31	0.45± 0.05	-
	at. [%]	10.42 ±0.11	63.90 ±0.33	-	1.09± 0.02	4.98± 0.04	11.50 ±0.06	-	1.44± 0.04	4.77± 0.05	-	1.85± 0.11	0.05± 0.01	-
S1	wt. [%]	22.85 ±0.11	65.01 ±0.32	-	-	1.99± 0.02	-	-	-	9.90± 0.05	-	-	-	0.26± 0.02
	at. [%]	30.24 ±0.15	64.59 ±0.32	-	-	1.17± 0.01	-	-	-	3.93± 0.02	-	-	-	0.07± 0.01
P2	wt. [%]	10.13 ±0.08	47.45 ±0.25	-	2.53± 0.03	5.34± 0.05	16.60 ±0.08	-	3.11± 0.07	10.58 ±0.11	-	2.80± 0.26	1.46± 0.11	-
	at. [%]	16.52 ±0.12	58.11 ±0.30	-	2.04± 0.02	3.88± 0.03	11.58 ±0.05	-	1.56± 0.03	5.17± 0.05	-	0.98± 0.09	0.15± 0.01	-
S2	wt. [%]	26.52 ±0.13	63.82 ±0.32	-	-	2.47± 0.02	0.19± 0.02	-	-	7.00± 0.05	-	-	-	-
	at. [%]	34.12 ±0.17	61.66 ±0.31	-	-	1.41± 0.01	0.11± 0.01	-	-	2.70± 0.02	-	-	-	-
P3	wt. [%]	7.44± 0.04	45.83 ±0.24	-	0.11± 0.01	0.18± 0.01	0.71± 0.01	-	-	42.54 ±0.19	-	2.77± 0.16	0.42± 0.03	-
	at. [%]	13.36 ±0.08	61.82 ±0.32	-	0.10± 0.01	0.15± 0.01	0.54± 0.01	-	-	22.90 ±0.10	-	1.07± 0.06	0.05± 0.01	-
S3	wt. [%]	8.95± 0.05	51.25 ±0.27	0.14± 0.01	-	0.14± 0.01	-	-	-	39.52 ±0.15	-	-	-	-
	at. [%]	15.07 ±0.09	64.76 ±0.34	0.11± 0.01	-	0.11± 0.01	-	-	-	19.94 ±0.08	-	-	-	-
P4	wt. [%]	5.81± 0.07	49.38 ±0.25	-	1.27± 0.02	8.10± 0.05	18.58 ±0.08	-	2.74± 0.06	8.62± 0.09	0.48± 0.04	4.47± 0.23	0.56± 0.04	-
	at. [%]	9.75± 0.12	62.20 ±0.31	-	1.05± 0.02	6.05± 0.04	13.33 ±0.06	-	1.41± 0.03	4.33± 0.04	0.20± 0.02	1.61± 0.08	0.06± 0.01	-
S4	wt. [%]	14.98 ±0.08	55.20 ±0.29	-	-	0.68± 0.02	-	-	-	29.14 ±0.12	-	-	-	-
	at. [%]	22.89 ±0.12	63.31 ±0.33	-	-	0.46± 0.01	-	-	-	13.34 ±0.06	-	-	-	-
P5	wt. [%]	6.89± 0.05	44.62 ±0.25	-	0.67± 0.02	0.79± 0.03	3.25± 0.04	0.30± 0.06	0.62± 0.03	37.94 ±0.19		4.43± 0.27	0.49± 0.18	-
	at. [%]	12.51 ±0.09	60.77 ±0.34	-	0.60± 0.02	0.64± 0.02	2.52± 0.03	0.21± 0.04	0.35± 0.01	20.63 ±0.10		1.73± 0.11	0.06± 0.02	-
S5	wt. [%]	17.73 ±0.09	58.81 ±0.29	-	-	0.25± 0.01	0.13± 0.01	-	0.11± 0.01	22.98 ±0.09	-	-	-	-
	at. [%]	25.71 ±0.13	64.02 ±0.32	-	-	0.16± 0.01	0.08± 0.01	-	0.05± 0.01	9.99± 0.04	-	-	-	-
P6	wt. [%]	4.58± 0.05	50.64 ±0.25	-	1.81± 0.02	9.54± 0.05	18.56 ±0.07	-	1.86± 0.04	2.74± 0.05	0.23± 0.03	9.42± 0.24	0.63± 0.04	-

		C	O	Na	Mg	Al	Si	P	K	Ca	Ti	Fe	Ir	Ni
	at. [%]	7.74± 0.08	64.23 ±0.31	-	1.51± 0.02	7.17± 0.04	13.41 ±0.05	-	0.97± 0.02	1.39± 0.03	0.10± 0.01	3.42± 0.09	0.07± 0.01	-
S6	wt. [%]	16.39 ±0.08	63.72 ±0.32	-	-	0.36± 0.01	-	-	-	19.52 ±0.09	-	-	-	-
	at. [%]	23.34 ±0.12	68.11 ±0.34	-	-	0.23± 0.01	-	-	-	8.33± 0.04	-	-	-	-
P7	wt. [%]	9.11± 0.06	62.50 ±0.28	-	-	-	0.21± 0.02	-	-	38.18 ±0.19	-	-	-	-
	at. [%]	15.16 ±0.09	65.64 ±0.35	-	-	-	0.15± 0.01	-	-	19.05 ±0.10	-	-	-	-
S7	wt. [%]	12.68 ±0.07	54.24 ±0.29	-	-	0.74± 0.02	-	-	-	32.34 ±0.14	-	-	-	-
	at. [%]	20.00 ±0.12	64.21 ±0.35	-	-	0.51± 0.01	-	-	-	15.28 ±0.07	-	-	-	-
P8	wt. [%]	5.58± 0.04	41.47 ±0.24	-	-	-	0.10± 0.02	-	-	52.86 ±0.25	-	-	-	-
	at. [%]	10.60 ±0.08	59.20 ±0.34	-	-	-	0.08± 0.02	-	-	30.12 ±0.14	-	-	-	-
S8	wt. [%]	13.51 ±0.08	59.66 ±0.31	-	-	0.43± 0.02	-	-	-	26.40 ±0.11	-	-	-	-
	at. [%]	20.35 ±0.11	67.45 ±0.35	-	-	0.29± 0.01	-	-	-	11.92 ±0.05	-	-	-	-

The elemental composition of pigment and shell samples (Table 1) highlighted the presence of iron (2.77-9.42 wt.%) and iridium (0.42-1.46 wt.%) in P1-P6 samples. The presence of Fe in samples confirms the brown-red color of the pigment. Even if the iridium is less present in the Earth's crust, it was discovered that this transition metal is abundant in the Cretaceous-Paleogene boundary (K/Pg) clays [39]. Taking into account the EDS data, the red pigments identified on shell samples can be a mixture of ochre (red ochre – hematite Fe_2O_3 and brown ochre – goethite FeO(OH)) [40]. The major elements such as carbon, oxygen, silicon, aluminum, calcium and potassium are present in all samples and are ussualy presented in aluminosilicates and kaolinites, named by Popelka-Filcoff and Zipkin as "accessory ochre minerals" [40].

Based on the EDS results, the principal component analysis and cluster analysis were carried out, both for pigments and shell samples (Figs 6 and 7).

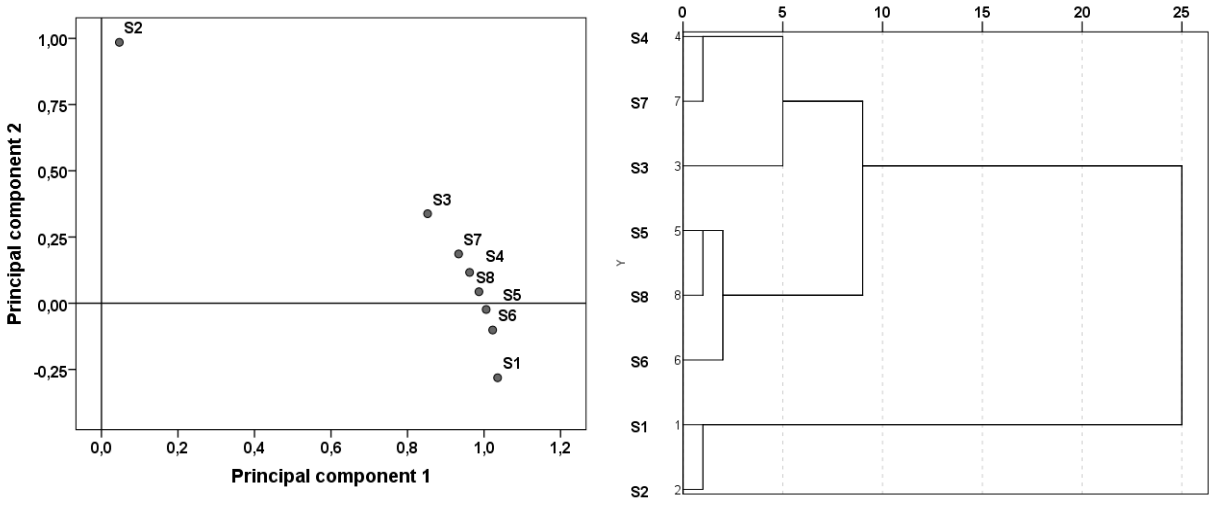

a) **b)**

Figure 6. Statistical analysis on elemental composition determined by EDS of shell samples: a) Principal component analysis (PCA); b) Cluster analysis (dendrogram) obtained using Average Linkage (Between Groups).

These methods allow sorting the studied samples in groups or clusters, based on their elemental content. The shell samples are characterized by similar elemental concentrations, except the sample S2. Regarding the pigment samples, it can be easily seen that two groups of samples are highlighted. The first cluster (P3, P5, P7, and P8) is characterized by high calcium content and low or missing iron and iridium content, meanwile the second cluster (P1, P2, P4, and P6) have lower Ca content and higher Fe and Ir content.

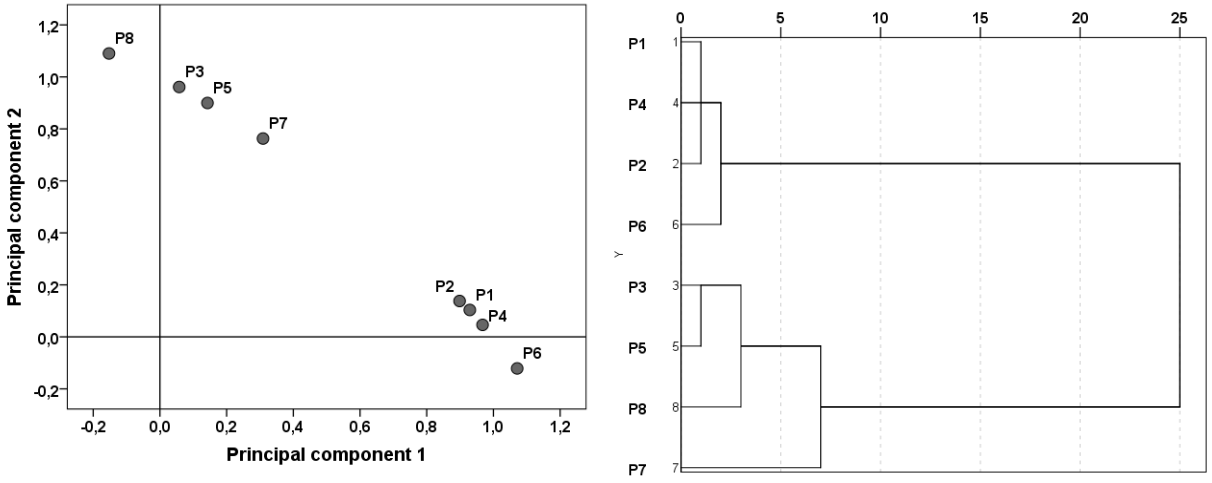

a) **b)**

Figure 7. Statistical analysis on elemental composition determined by EDS of pigment samples: a) Principal component analysis (PCA); b) Cluster analysis (dendrogram) obtained using Average Linkage (Between Groups).

The tentative assignments and relative intensity regarding FTIR spectra are presented in Table 2. It is well known [41-43] that quite enough inorganic pigments have characteristic absorptions in the low wavenumber range, being frequently associated with red natural pigments, including red lead, cinnabar, hematite or even ochre, cadmium red, and so on, which don't have characteristic absorption in mid-IR region. Withal, the ATR-FTIR usefulness in the region 600-300 cm^{-1} for investigation of inorganic pigments of shell was demonstrated in a couple of cases [44, 45]. Alongside of mineral constituents (e.g., hydroxyapatite, calcite), in near and mid-infrared regions can be identified the most abundant structural protein of shell, which is β-keratin [46]. The constituents of this insoluble protein are C, O, N, H, Ca, P and S and that are sustain by EDS analysis (Table 1), as well as by ATR-FTIR (Table 2). *β*-Keratin from the composition of shell is identically in composition with the one from hair and nail. According with study of Wang et al. (2016) [46], the structure of shell is defined as a natural polymer (i.e., it exceeds about 1,000 atoms in length), which means long chains of organic molecules (named each of them as monomer), with a high molecular weight.

From Table 2, for the samples S1a - S5a, it can see that the absorption around 1640 cm^{-1}, 1445 cm^{-1} and 1240 cm^{-1} can be attributed to amide group (i.e., -CO-NH-) of proteins from β-keratin. These bands are called amide bands [47, 48] and correlated to the C-O stretch, N-H bend, and C-N stretch, respectively. Also, the medium peaks from 1403 to 1415 cm^{-1} (e.g., S1-S5), correspond to the C-H band of keratin structure.

Table 2. FTIR data [cm^{-1}] and relative intensity *(s – strong, m- medium, w - weak)* of shell samples with tentative assignments.

Sample	Characteristic bands wavenumbers [cm^{-1}]	Relative Intensity	IR ν_{max} [cm^{-1}] (Vibration mode)	Organic/inorganic compound/pigment
P1	1442/1415/1018/961/872/600/560/468/355	w/m/s/w/m/m/s/w/ w	1442 (Amide band, N-H bend); 1415 (C-H bend); 1018, 872; 600, 560 (true fingerprint region); 560-354 (Si-O)	Keratin structure; red ochre (Fe_2O_3); silica
S1	1445/1413/1019/960/871/711/600/560/468/436/361	m/m/s/w/m/w/m/s/w/w/m	1445 (Amide band, N-H bend); 1413 (C-H bend); 1013, 871; 711, 600, 560 (true fingerprint region); 560-354 (Si-O)	Keratin structure; hydroxyapatite ($Ca_3(PO_4)_5(OH)$); silica
P2	1630/1412/997/871/798/779/682/597/498/459/421/381/363	w/m/s/m/w/w/w/w/w/w/m/w/w	1630 (Amide band, C-O stretch, and O-H bend); 1412 (C-H bend); 997, 871; 779, 600, 559-354 (Si-O band)	Keratin structure; red ochre (Fe_2O_3); pigment (Fe_2O_3+MnO_2+$SiO_2 \cdot Al_2O_3$);
S2	1403/1011/869/713/600/556/470/390/369/360	s/s/s/m/m/s/w/w/w/s	1403(C-H bend); 1012, 871; 711, 600, 559 (true fingerprint region); 560-354 (Si-O band);	Keratin structure; hydroxyapatite ($Ca_3(PO_4)_5(OH)$); silica
P3	2360/1638/1414/1019/872/601/560/464//355	w/w/m/s/m/w/s/m/ w/m	2360 (C-H stretch); 1638 (Amide band, C-O stretch, and O-H bend); 1414 (C-H bend); 1019, 872; 601,560-354 (Si-O)	Keratin structure; red ochre (Fe_2O_3); silica
S3	1642/1407/1240/1012/869/691/600/559/377/356	m/m/w/s/m/w/m/w/w/w/	1642 (Amide band, C-O stretch, and O-H bend); 1407 (C-H bend); 1240 (amide band, C-N stretch); 1012, 871; 711, 600, 559 (true fingerprint region); 560-354 (Si-O band)	Keratin structure; hydroxyapatite ($Ca_3(PO_4)_5(OH)$); silica
P4	2360/2341/1633/1413/1019/871/601/560/469/392/380	w/w/w/m/s/m/m/s/w/w/s	2360 (C-H stretch); 1633 (Amide band, C-O stretch, and O-H bend); 1413 (C-H bend); 1012, 871; 711, 600, 559 (true fingerprint region); 560-354 (Si-O band)	Keratin structure; red ochre (Fe_2O_3); TiO_2 white rutile pigment; silica
S4	1633/1408/1241/1007/872/711/597/559/468/457/408/389/366/354	m/s/w/s/m/w/w/s/w/w/w/w/s/s	1633(Amide band, C-O stretch, and O-H bend); 1408 (C-H bend); 1241 (amide band, C-N stretch); 1012, 871; 711, 600, 559 (true fingerprint region); 560-354 (Si-O band)	Keratin structure; hydroxyapatite ($Ca_3(PO_4)_5(OH)$); silica
P5	1637/1410/1016/870/600/559/469/431/401/388/379/365	m/m/s/m/m/s/w/w/w/w/w/s	1637(Amide band, C-O stretch, and O-H bend); 1410 (C-H bend); 1012, 871; 711, 600, 559 (true fingerprint region); 560-354 (Si-O band)	Keratin structure; red ochre (Fe_2O_3); silica
S5	1640/1409/1236/1012/960/871/601/560/468/441/416/386/360	m/m/w/s/w/m/m/s/w/w/w/w/s	1640 (Amide band, C-O stretch, and O-H bend); 1409 (C-H bend); 1236 (amide band, C-N stretch); 1012, 871; 711, 600, 559 (true fingerprint region); 560-354 (Si-O band)	Keratin structure; hydroxyapatite ($Ca_3(PO_4)_5(OH)$); silica
P6	1630/1412/997/871/798/779/682/597/498/459/421/381/363	w/m/s/m/w/w/w/w/w/w/m/w/w	1630 (Amide band, C-O stretch, and O-H bend); 1412 (C-H bend); around 1410, 1012, 871; 711, 600, 559 (true fingerprint region); 560-354 (Si-O band)	Keratin structure; red ochre (Fe_2O_3); yellow ochre ($FeO(OH)$+$SiO_2 \cdot Al_2O_3$); TiO_2 white rutile pigment; silica
S6	1416/1018/889/716/600/557/470/360	s/s/s/m/m/s/w/s	1416(C-H bend); 1018, 889; 716, 600, 559 (true fingerprint region); 560-354 (Si-O band);	Keratin structure; hydroxyapatite ($Ca_3(PO_4)_5(OH)$); silica
P7	2369/1633/1410/1011/872/601/560/464/426/355	w/w/m/s/m/w/s/m/w/ m	2360 (C-H stretch); 1633 (Amide band, C-O stretch, and O-H bend); 1410 (C-H bend); 1011, 872; 601, 560-354 (true fingerprint region);	Keratin structure; red ochre (Fe_2O_3); silica
S7	1642/1410/1244/1012/869/691/600/559/468/393/377/356	m/m/w/s/m/w/m/w/w/w/w/w	1642 (Amide band, C-O stretch, and O-H bend); 1410 (C-H bend); 1244 (amide band, C-N stretch); 1012, 869; 691, 600, 559 (true fingerprint region); 560-354 (Si-O band)	Keratin structure; hydroxyapatite ($Ca_3(PO_4)_5(OH)$); silica
P8	1639/1412/997/871/798/779/682/597/498/459/421/381/363	w/m/s/m/w/w/w/w/w/w/m/w/w	1639 (Amide band, C-O stretch, and O-H bend); 1412 (C-H bend); around 1410, 1012, 871; 711, 600, 597-363 (true fingerprint region);	Keratin structure; red ochre (Fe_2O_3); yellow ochre ($FeO(OH)$+$SiO_2 \cdot Al_2O_3$); silica
S8	1413/1015/872/710/600/560/470/390/369/360	s/s/s/m/m/s/w/w/w/s	1413(C-H bend); 1015, 872; 710, 600, 560 (true fingerprint region); 560-354 (Si-O band); 560-354 (Si-O band)	Keratin structure; hydroxyapatite ($Ca_3(PO_4)_5(OH)$); silica

The broad, complex band between 1000 and 400 cm^{-1} has been called the "true fingerprint region" of proteins [47], because it is more characteristic of protein-based substances. Strong bands around 1012 cm^{-1}, medium bands at 871 cm^{-1}, week band around 711 cm^{-1}, medium bands at 600 cm^{-1} and strong bands around 560 cm^{-1} were characteristic for shell sample (*i.e*., true fingerprint region, Table 2). The presence of inorganic pigments was observed by both techniques, EDS and FTIR. Thus, the signals from 779 and 798 cm^{-1} and between 363 and 597 cm^{-1} (Table 2) are related to SiO vibrations mainly from silica. The red pigments observed on the surface of samples are probably red ochre (Fe_2O_3) or mixture of red and yellow ochre, while white rutile pigment (TiO_2) is identified on sample P4 and P6.

4. CONCLUSIONS

Related to archaeological records, we found that such pigment residues do not appear at none of the *Unio* valves used for processing ceramics or in the functional scratches present on the edge contour. They appear in the form of spots especially on the exterior side. In this respect, it could advance the hypothesis of using the dorsal face of the valve to break the nucleus pigments but red spots do not associate with a flattened surface and use-wear strations resulting from the friction of this type of material. In addition, it could invoke the use of valves as containers but a mixture of ocher and other substances would have led to the appearance of the internl side of the deeper scratches with random orientation [49]. Instead, the microscope analysis revealed other patterns of use-wear on the internal side which seem to be related to the rubbing of the nacre layer with fingers. From the chemical point of view (EDS data), the shell samples are similar, meanwhile the pigment samples are splitted in two clusters/groups. The spectral data allowed to identify the presenece of keratin (all samples), hydroxyapatite (all shell samples), red and yellow ochre, white rutile pigment etc.

REFERENCES

[1] Marie, B., Luquet, G., Pais De Barros, J.-P., Guichard, N., Morel, S., Alcaraz, G., Bollache, L., Marin F., *FEBS J.*, **274**, 2933, 2007.
[2] Bøggild, O., *The shell structure of the mollusks*, A.F. Host, Kjobenhavn, 1930.
[3] Furuhashi, T., Schwarzinger, C., Miksik, I., Smrz, M., Beran, A., *Comp. Biochem. Physiol. Part B: Biochem. Mol. Biol.*, **154**, 351, 2009.
[4] Sturm, C.F., Pearce, T.A., Valdes, A. (Eds.), *The Mollusks: A guide to their Study, Collection, and Preservation*, American Malacological Society, Pittsburgh, 2006.
[5] Agbaje, O.B.A., Shir, I.B., Zax, D.B., Schmidt, A., Jacob, D.E., *Acta Biomater.*, **80**, 176, 2018.
[6] Song, F., Soh, A.K., Bai, Y.L., *Biomater.*, **24**(20), 3623, 2003.
[7] Marin F., Marie B., Ben Hamada S., Ramos-Silva P., Le Roy N., Guichard N., Wolf S.E., Montagnani C., Joubert C., Piquemal D., Saulnier D., Gueguen Y., "Shellome": proteins involved in mollusk shell biomineralization – diversity, functions. In Watabe, S., Maeyama, K., Nagasawa, H. (Eds.), *Recent Advances in Pearl Research*, TerraPub, Tokyo, pp. 149-166, 2011.
[8] Levi-Kalisman Y., Falini G., Addadi L., Weiner S., *J. Struct. Biol.*, **135**, 8, 2001.
[9] Agbaje, O.B.A., Thomas, D.E., Mclnerney, B.V., Molloy, M.P., Jacob, D.E., *Mar. Biol.*, **164**, 208, 2017.

[10] Wu, Z., Zhao, D., *Chem Commun*., 47, 3332, 2011.
[11] Elwakeel, K., Elgarahy, A., Mohammad, S., *J. Environ. Chem. Engin.*, **5**, 578, 2017.
[12] Mutvei, H., Westermark, T., How environmental information can be obtained from Naiad shells. In Bauer, G., Wächtler, K. (Eds.), *Ecology and Evolution of the Freshwater Mussels Unionoidea. Ecological Studies*, Vol. 145. Springer, Berlin & Heidelberg, pp. 367-379, 2001.
[13] Roopnarine, P.D., Fitzgerald, P., Byars, G., Kilb, K., *PALAIOS*, **13**, 395, 1998.
[14] Carroll, M., Romanek, C., Paddock L., *Chem. Geol.*, **234**, 211, 2006.
[15] Thébault, J., Chauvaud, L., L'Helguen, S., Clavier, J., Barats, A., Jacquet, A., Pécheyran, C., Amouroux, D., *Limnol. Oceanogr*., **54**, 1002, 2009.
[16] Schöne, B.R., Surge, D., *Treatise Online*, **46**, 1, 2012.
[17] Schöne, B.R., Fiebig, J., Pfeiffer, M., Gleß, R., Hickson, J., Johnson, A.L.A., Dreyer, W., Oschmann, W., *Palaeogeogr. Palaeoclimatol. Palaeoecol.*, **228**, 130, 2005.
[18] Schöne, B.R., Oschmann, W., Tanabe, K., Dettman, D., Fiebig, J., Houk, S.D., Kanie, Y., *Quaternary Sci. Rev.*, **23**, 1137, 2004.
[19] Wegst, U.G.K., Bai, H., Saiz, E., Tomsia, A.P., Ritchie, R.O., *Nature Mater.*, **14**, 23, 2015.
[20] Deville, S., Saiz, E., Nalla, R.K., Tomsia, A.P., *Science*, **311**, 515, 2006.
[21] Niebel, T.P., Bouville, F., Kokkinis, D., Studart, A.R., *J. Mech. Phys. Solids*, **96**, 133, 2016.
[22] Dunlop, J.W.C., Fratzl, P., *Annu. Rev. Mater. Res.*, **40**, 1, 2010.
[23] Haag, W.R., Rypel, A.L., *Biol. Rev. Camb. Philos. Soc.*, **86**(1), 225, 2011.
[24] Voinea, V., Dobrinescu, C., *Pontica*, **35**(36), 9, 2002-2003.
[25] Voinea, V., Neagu, G., *Studii de Preistorie*, **3**, 149, 2006.
[26] Philipp, E.E.R., Abele, D., *Gerontology*, **56**, 55, 2009.
[27] Wanamaker, A.D.J., Heinemeier, J., Scourse, J.D., Richardson, C.A., Butler, P.G., Eiríksson, J., Knudsen, K.L., *Radiocarbon*, **50**, 399, 2008.
[28] Arslanov, K.A., Tertychnaya, T.V., Chernov, S.B., *Radiocarbon*, **35**(3), 393, 1993.
[29] Keith, M.L., Anderson, G.M., *Science*, **141**(3581), 634, 1963.
[30] Voinea, V., Dobrinescu, C., Neagu, G., Bălăşescu, A., Radu, V., *Europ. Archaeol.*, **26**, 10-11, 2006/2007.
[31] Voinea, V., Neagu, G., *Pontica*, **XLI**, 9, 2008.
[32] Bălăşescu, A., Radu, V., *Pontica*, **33-34**, 25, 2003.
[33] Bălăşescu, A., Radu, V., Oameni și animale. Strategii și resurse la comunitățile preistorice Hamangia și Boian. In: *Biblioteca Muzeului Național, Seria Cercetări Pluridisciplinare*, Vol. 9, Editura Cetatea de Scaun, București, p. 310, 2004.
[34] Bălăşescu, A., *Pontica*, **41**, 49, 2008.
[35] Radu, V., *Pontica*, **41**, 57, 2008.
[36] Tornero, C., Balasescu, A., Ughetto-Monfrin, J., Voinea, V., Balasse, M., *J. Archaeol. Sci.*, **40**, 4039, 2013.
[37] Mărgărit, M., Radu, V., Voinea V., *Eur. J. Archaeol.*, **24**(2), 180, 2021.
[38] Debruyne, S., *Environ. Archaeol.*, **19**(2), 153, 2014.
[39] Prakash, J., Ahmad, S.M., *Cretaceous Res.*, **29**(4), 592, 2008.
[40] Popelka-Filcoff, R.S., Zipkin, M., *J. Archaeol. Sci.*, **137**, 105530, 2022.
[41] Vahur, S., Teearu, A., Leito, I., *Spectrochim. Acta A*, **75**, 1061, 2010.
[42] Schrader, B., *Infrared and Raman Spectroscopy: Methods and Applications*, VCH, Weinheim, 1995.
[43] Smith, B., *Infrared Spectral Interpretation: A Systematic Approach*, CRC Press, Boca Raton, 1999.

[44] Davis, S.P., Abrams, M.C., Brault, J.W., *Fourier Transform Spectrometry*, Academic Press, San Diego, 2001.
[45] Hofmeister, A.M., Keppel, E., Speck, A.K., *Monthly Notices Royal Astron. Soc.*, **345**, 16, 2003.
[46] Wang, B., Yang, W., McKittrick, J., Meyers, M.A., *Progr. Mater. Sci.*, **76**, 229, 2016.
[47] Naumann, D., Infrared Spectroscopy in Microbiology. In Meyers R.A. (Ed.), *Encyclopedia of Analytical Chemistry*, John Wiley & Sons, Chichester, pp. 102-131, 2000.
[48] Barbes, L., Radulescu, C., Stihi, C., *Rom. Rep. Phys.*, **66**(3), 765, 2014.
[49] Manca, L. *Anthropozoologica*, **51**(2), 144, 2016.